Molecular Dynamics and NMR Study of the α(1→4) and α(1→6) Glycosidic Linkages: Maltose and Isomaltose

Robert B. Best, Graham E. Jackson, and Kevin J. Naidoo*

Department of Chemistry, University of Cape Town, Rondebosch 7701, South Africa

Received: November 7, 2000; In Final Form: February 26, 2001

We report the results of molecular dynamics (MD) simulations compared with NMR relaxation experiments for maltose and isomaltose. The (Φ,Ψ) adiabatic map for maltose shows a single principal energy well, while the (Φ,Ψ,Ω) map of isomaltose reveals multiple low energy minima separated by significant barriers (9 kcal/mol) in some cases. The greater accessible conformational space of the α(1→6) linkage appears to make it more flexible as compared with the α(1→4) linkage, especially in the presence of water. Correlation times for glycosidic dihedral angle fluctuations are significantly shorter in the case of isomaltose. While the generalized order parameters calculated from the simulations do not show a large difference in the spatial restriction of the motion, they are nonetheless generally lower for isomaltose. The time scales of the overall rotational motion (τ_M) and the local molecular motion (τ_e) are similar for both maltose and isomaltose. This makes reliable estimates of order parameters from experimental relaxation data (using the *model-free* formalism) unfeasible. We were, however, able to show that T_1 relaxation times calculated from the MD data agree well with the experimental values. As a further measure of solution flexibility, three-dimensional water distributions were calculated about each disaccharide. These demonstrate that the more rigid maltose solute causes the water to adopt a more localized structure about it. Because of its extended structure, isomaltose appears to make a greater number of hydrogen bonds to water.

1. Introduction

The conformation of oligosaccharides composed of glucopyranosyl monomers is largely determined by rotation about the glycosidic linkage dihedrals. Examples of such carbohydrates are found in small oligosaccharides and glycoconjugates involved in cellular signaling and recognition,[1] structural carbohydrates such as cellulose and the components of starch granules, involved in storage. The two components of starch are described by only two kinds of linkage: amylose is a simple α(1→4)-linked linear glucose polymer, while amylopectin comprises short α(1→4)-linked chains with α(1→6) branches approximately every 30 residues. Amylose is found to be less soluble in water than amylopectin, a property that is often explained in terms of an assumed difference in flexibility between the α(1→4)- and α(1→6) linkages.[2] This is significant when attempting to develop starch products as replacements for conventional polymer materials.[3,4]

The structural characterization of amorphous starch is a challenge for existing experimental methods, due to the lack of ordered structure. Crystal structures have only been accessible for a few small oligosaccharides,[5−7] and while such studies have been useful, they do not give information on solution structure or dynamics. On a larger scale, detailed studies of the glucopyranosyl hexamer,[8] fiber-diffraction studies,[9,10] and X-ray microfocus diffraction methods[11] have provided insights into the structure of amorphous starch. Atomic force microscopy on starch granules has also been used to get low resolution structural information.[12]

High-resolution NMR spectroscopy holds the most promise for studying carbohydrate conformations and dynamic properties in solution. Vicinal coupling constants give information on dihedral angles via the Karplus relationship. These have proved valuable in determining the distribution of hydroxymethyl rotamers,[13−15] and $^3J_{C,H}$ couplings contain information on conformation at a glycosidic dihedral. The nuclear Overhauser effect (nOe) can be used to give interresidue distances, but the interpretation of such measurements is complicated by conformational averaging on the NMR time scale and the limited number of observable nOe's between residues.[1,16,17] In such cases, molecular dynamics (MD) simulations have been useful in reconciling the data with multiple conformations,[18−22] demonstrating the flexibility in many glycosidic linkages.[23]

The most common method for extracting specific motional information from NMR relaxation data is the *model-free* formalism,[24,25] originally developed for proteins. However, this method has limited applicability to smaller molecules such as oligosaccharides, due to problems in fitting the *model-free* parameters. Molecular dynamics (MD) simulation data, however, provide a level of atomistic detail that allows unambiguous characterization of molecular motion. Correlation functions for glycosidic dihedrals and molecular tumbling provide a description of the saccharide motion. In addition, any number of experimental measurables may be calculated from the MD trajectory; for example, *model-free* parameters may readily be evaluated in this way. Of particular interest here is the direct calculation of the NMR relaxation times from the simulation data that allow for comparison with the values produced from experiment. In this paper, we compare the dynamical properties and solute−solvent interactions of the α(1→4) and α(1→6) linkages using molecular dynamics simulations on maltose (α-(1→4) linkage) and isomaltose (α(1→6) linkage). As a check on the simulation and force-field, experimentally determined

* To whom correspondence should be addressed. E-mail: knaidoo@psipsy.uct.ac.za. Fax: +27-21-689-7499.

10.1021/jp0040704 CCC: $20.00
Published on Web 05/01/2001

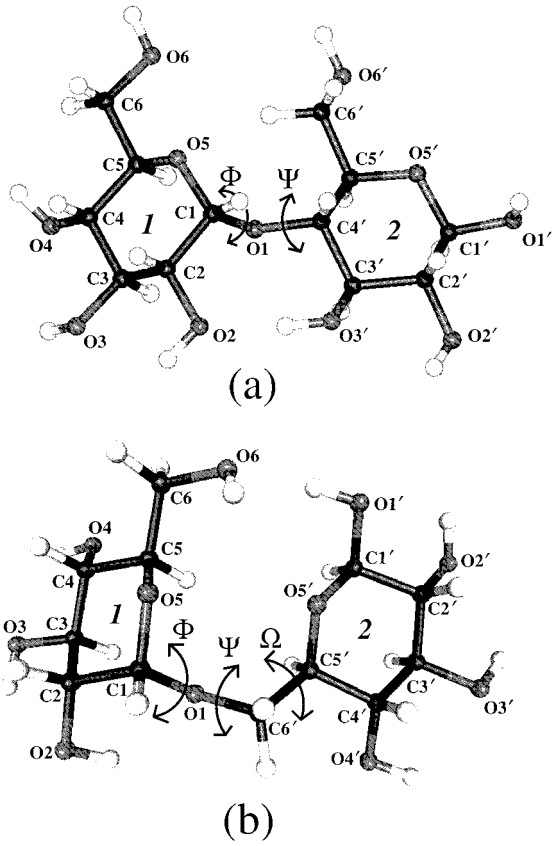

Figure 1. Definition of names for atoms and glycosidic torsion angles for (a) β-maltose and (b) β-isomaltose. In each case, the atoms names follow the standard glucosyl convention, with those in the reducing residue (on the right) being distinguished by primes. The nonreducing and reducing residues are referred to as residue 1 and 2, respectively.

T_1 relaxation times are compared with those calculated from simulation.

2. Theory and Simulation

Schematic structures for maltose and isomaltose are depicted in Figure 1, showing the names used for the non-hydrogen atoms and the dihedral angles. The interresidue dihedrals (Φ,Ψ) for maltose are defined as Φ: H1−C1−O1−C4′ and Ψ: C1−O1−C4′−H4′ according to previous convention,[26,27] while for isomaltose they are defined by the heavy atoms as Φ: O5−C1−O1−C6′, Ψ: C1−O1−C6′−C5′, and Ω: O1−C6′−C5′−C4′. The orientation of the hydroxymethyl groups is in general given by Θ: C4−C5−C6−O6, the two in maltose being distinguished by the prime notation. The three gauche conformers of the hydroxymethyl groups are specified by the standard two character notation in which the first character, either *g* or *t* denotes whether the dihedral O5−C5−C6−O6 is *gauche* or *trans* and the second character describes the C4−C5−C6−O6 dihedral. The three possible orientations are thus denoted *gg*, *gt*, and *tg*.

All calculations were done using the recent carbohydrate force-field of Palma et al. implemented in CHARMM,[29] which will be referred to here as the PHLB force-field to distinguish it from the earlier HGFB force-field of Ha et al.[30] The new parameter set addresses the excessive flexibility in the earlier force-field, and the incorrect preference of the primary alcohols in that force field for adopting the *tg* rotamer.[14] The TIP3P model,[31,32] which has been used extensively in explicit solvent simulations with this force field, was used to represent water.

NMR Relaxation Parameters. Carbon-13 NMR relaxation parameters for carbohydrates, such as the longitudinal relaxation time, T_1, are mainly dependent on the dipolar relaxation between a given carbon and its directly attached proton, if chemical shift anisotropy (CSA) may be neglected. Specifically, if the C−H vector is denoted μ_{LF}, then the relaxation is described by the time correlation function (TCF) in eq 1, where P_2 is the second-order Legendre polynomial $^1/_2(3x^2 - 1)$. The relaxation parameters are a function of the spectral density, $J(\omega)$, of this correlation function (eq 2). T_1 and T_2 may then be calculated

$$C(t) = \frac{1}{5}\langle P_2(\mu_{LF}(0) \cdot \mu_{LF}(t))\rangle \quad (1)$$

$$J(\omega) = \int_0^\infty C(t) \cos \omega t dt \quad (2)$$

from the spectral density via eqs 3 and 4, respectively, as a function of the Larmor frequencies for hydrogen (ω_H) and carbon (ω_C). Thus, although information about the C−H vector motion is contained in the experimental T_1 values, the most that can be deduced from experimental relaxation data is the form of the spectral density function, if, for example, T_1 and T_2 are measured at several magnetic field strengths.

$$T_1^{-1} = \frac{1}{4}D^2[J(\omega_H - \omega_C) + 3J(\omega_C) + 6J(\omega_H + \omega_C)] \quad (3)$$

$$T_2^{-1} = \frac{1}{8}D^2[4J(0) + J(\omega_H - \omega_C) + 3J(\omega_C) + 6J(\omega_H) + 6J(\omega_H + \omega_C)] \quad (4)$$

where $D = \hbar\gamma_C\gamma_H\langle r^3\rangle^-1$.

The most frequently used method of experimentally characterizing the spectral density is the model-free formalism[24,25] shown in eq 5, which fits three motional parameters to the experimental data: τ_M is the *overall rotational correlation time* for the whole molecule, τ_e is the *effective correlation time* describing the local time scale of motion, and S^2 is the *generalized order parameter*, related to the spatial restriction of local motion. These parameters may be obtained by a least-squares fit of the relaxation data to this target function.

$$J(\omega) = \frac{2}{5}\left(\frac{S^2\tau_M}{1 + (\tau_M\omega)^2} + \frac{(1 - S^2)\tau}{1 + (\tau\omega)^2}\right) \quad (5)$$

where $\tau^{-1} = \tau_M^{-1} + \tau_e^{-1}$.

The fit of the *model-free* spectral density to experimental data produces the truest fit to the actual parameters (when these are known from a model) when the internal and overall motions are on different time scales (i.e. $\tau_e < 0.1\tau_M$). If τ_e is of similar magnitude to τ_M, the fit is very insensitive to the value of τ_e, making a valid fit to the data difficult.

Parameters from MD Trajectories. Generalized order parameters S^2 may be directly calculated from simulation using the definition used to derive eq 5,[25] resulting in eq 6. Here the

$$S^2 = \lim_{t\to\infty} C(t) = \frac{5}{4\pi}\sum_{m=-2}^{2} |\langle Y_{2m}(\theta_{mol},\phi_{mol})\rangle|^2 \quad (6)$$

$Y_{2m}(\theta,\phi)$ are the standard second order spherical harmonic functions. This provides a method of calculating order parameters, and hence describing the motion, which does not depend on the validity of an experimental fit. In addition, it provides a method of validating a simulation, by comparing simulated and experimentally determined order parameters; this remains an indirect comparison, as it depends on the reliability of the model-

free fit to the NMR data. When the aim is to benchmark a simulation against experimental data, it may be better to calculate the relaxation parameters such as T_1 directly. This could be done using eqs 1−3; however, in general, molecular dynamics simulations with explicit solvent are too short to represent accurately the long-term decay to zero of the correlation function in eq 1. If, however, the correlation function for the internal motions (eq 1 calculated within the molecular reference frame) is considered to have decayed to a steady state within the time of the simulation (a few hundred picoseconds), it is possible to factor the correlation function (eq 1) into internal and overall contributions. The correlation function may then be evaluated by eq 7, which uses some estimate of the overall rotational correlation time τ_M to calculate the overall contribution using an exponential decay $C_0(t) = \exp(-t/\tau_M)$ and the actual internal correlation function $C_I(t)$ calculated from eq 1 using the trajectory data, but oriented to remove the overall rotation.

$$C(t) = \begin{cases} C_I(t)\exp(-t/\tau_M) & \text{for } t \le t_{max} \\ C_I(t_{max})\exp(-t/\tau_M) & \text{for } t > t_{max} \end{cases} \quad (7)$$

In this expression, the internal correlation function is considered to have decayed to zero after time t_{max} [chosen from consideration of the decay of $C(t)$ for the C−H vectors when the dynamics coordinates are oriented to a reference structure to remove the effect of molecular tumbling].[33]

Adiabatic Maps. Prior to running MD simulations, the energy landscape of each disaccharide was investigated by means of an adiabatic vacuum map, to identify significant minima likely to be sampled during the dynamics. These were constructed using an adaptation of the simulated annealing algorithm,[34] similar to that previously applied to other disaccharides.[35] The calculation of the maltose map by this method has been described previously.[36] The isomaltose map was constructed in three-dimensional (Φ,Ψ,Ω) space using a search grid of 20° and a three phase search. In the first step, simulated annealing at each grid point (with the glycosidic dihedrals constrained to the grid values)[35] generated an approximate map that was used to identify five important minima for each section in Φ. Ring dihedrals were constrained during heating to their equilibrium values to prevent ring flipping to boat and twist conformers. The structures and energies of the chosen minima were refined in the second step by means of a further 30 cycles of simulated annealing, and the lowest energy structure was picked from each of these runs. For the last step, the refined minima were used as starting structures at each grid point, with their glycosidic dihedrals edited to the appropriate value. The final structure was chosen as the lowest energy conformation out of these minimized structures and the structure determined in the initial rough map.

Simulation Conditions. All simulations were performed in the microcanonical ensemble (constant N, V, E) using the leapfrog Verlet dynamics integrator; this ensemble was chosen to avoid the effects of temperature reassignment on the long-term values of time correlation functions. In each case, the system was initially heated and equilibrated in the canonical ensemble at 300 K, and the temperature was found to fluctuate about this value throughout the simulation. The molecular dynamics program CHARMM was used for all the simulations.

Both maltose vacuum and solution simulations were started from the saddle point (0,0) between the two major energy wells on the adiabatic map.[36] The vacuum simulation was heated from 50 to 300 K over 12.5 ps and equilibrated at 300 K for a further 12.5 ps, with constraints on both the intra-ring and glycosidic dihedral angles, to prevent transitions to the boat conformer, and to maintain the initial (0,0) conformation. The system was run for 1 ns in the microcanonical ensemble using the leapfrog verlet integrator, without glycosidic constraints. For the solution simulation, maltose was solvated using 488 explicit TIP3P water molecules in a cubic cell of side 24.6433 under periodic boundary conditions, to give a density of 1.0037 g/cm^3. The system was heated from 100 to 300 K over 20 ps and equilibrated for 50 ps, using velocity reassignment to control the temperature. Dynamics data were generated over a period of 1.5 ns in the microcanonical ensemble with the temperature stable at 300 K. Interresidue dihedrals were constrained to (0,0) during heating and equilibration. As maltose has already been extensively studied,[26,27,36,37] one simulation in a vacuum and one in solution were considered sufficient for our purposes.

On the basis of the three-dimensional adiabatic map, the six lowest lying minima were chosen as starting points for vacuum simulations of isomaltose, and the three lowest for solution simulations. The conformation corresponding to the crystal structure of panose[6,7] is also effectively included among the starting structures, since it falls within the global minima on the adiabatic map. Simulation conditions were identical to those for maltose, except that a truncated octahedral water box of side 36.9953 Å was used with appropriate boundary conditions and the solution simulations were carried out for 2 ns.

3. NMR Experimental Details

Values of T_1 and T_2 for maltose in D_2O were taken from previously published data.[38] Isomaltose (Sigma) was dissolved in 99.9% deuterated ^2H_2O. The ^{13}C assignment used was that previously published,[39] but the assignment of the reducing terminus C1 anomers was reversed based on the ratio of their peak heights. Two peaks were observed for all of the carbons on the reducing residue and some on the nonreducing residue due to the two anomeric forms of the reducing ring, although in some cases this was only visible at higher fields. Carbon-13 T_1 relaxation data were measured at 298 K on 200, 300, and 400 MHz Varian spectrometers, using a standard inversion−recovery pulse sequence. The errors in the exponential fits were in all cases less than 10%. The T_1 relaxation times for the β-anomer of isomaltose at the three frequencies are available as supplementary data.

4. Motional Properties

We use maltose and isomaltose as models to investigate the flexibility of $\alpha(1\rightarrow4)$ and $\alpha(1\rightarrow6)$ linkages in larger carbohydrate polymers. Specifically, we are interested in whether there are differences in the rate or extent of motion about the different glycosidic linkages, and in the relative rates of internal and overall motion.

Ideally, a motional description of each disaccharide based entirely on experimental NMR data should be possible using a method such as the *model-free* formalism. Indeed, this approach has been applied before to oligosaccharides and cyclodextrins. In the application to sucrose,[40] the second term of the *model-free* spectral density was neglected based on the assumption that $\tau_M \gg \tau_e$. Furthermore, in the analysis of other mono- and disaccharides and cyclodextrins,[41,42] it was necessary to set $\tau_e = 0$ to obtain physically sensible fitted values for S^2 and τ_M. This does not mean that τ_e is in fact very short, as motions about the glycosidic dihedrals on the same time-scale as the overall tumbling would not be detected in the fit to τ_e.[42] Recent molecular dynamics simulations of sucrose have suggested that the correlation times for internal and overall motion are actually very similar.[21]

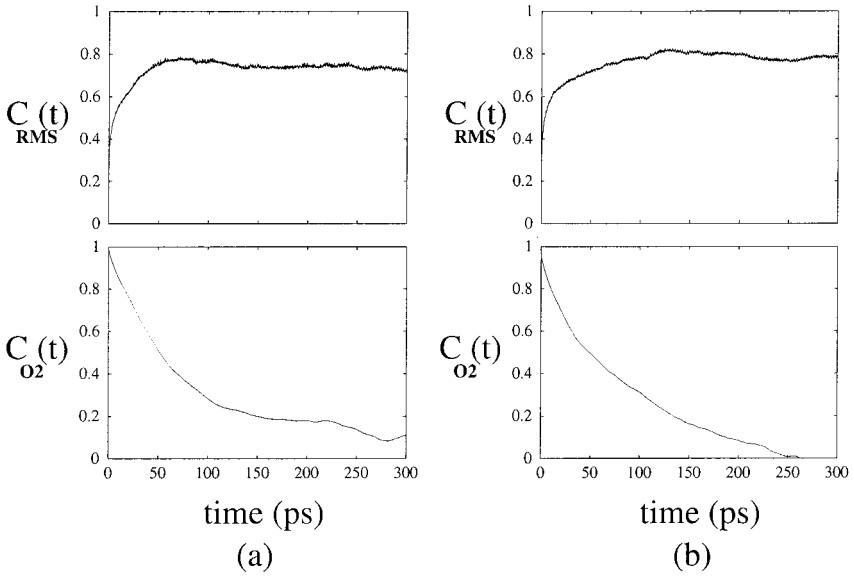

Figure 2. RMS fit autocorrelation functions, $C_{RMS}(t)$, (internal motion) and second-order orientational autocorrelation functions, $C_{O2}(t)$, for (a) maltose and (b) isomaltose in solution.

TABLE 1: Order Parameters for Maltose and Isomaltose Calculated from Simulation and from Experimental Relaxation Parameters (using $t_e = 0$ and $t_M = 0.1$ ns for Both)

	C1	C2	C3	C4	C5	C6	C1′	C2′	C3′	C4′	C5′	C6′
						Maltose						
S^2 (sim)	0.88	0.93	0.92	0.92	0.92	0.83	0.84	0.84	0.84	0.86	0.85	0.80
S^2 (expt)	0.89	0.88	0.92	0.99	0.92	0.77	0.73	0.75	0.74	0.82	0.75	0.86
						Isomaltose						
S^2 (sim A)	0.81	0.77	0.76	0.76	0.77	0.81	0.64	0.63	0.62	0.63	0.66	0.67
S^2 (sim B)	0.87	0.84	0.83	0.84	0.85	0.84	0.87	0.86	0.88	0.89	0.90	0.85
S^2 (sim C)	0.85	0.81	0.80	0.80	0.82	0.76	0.74	0.73	0.73	0.74	0.76	0.67
S^2 (sim ave)	0.84	0.81	0.80	0.80	0.81	0.80	0.75	0.74	0.75	0.75	0.77	0.73
S^2 (expt)	0.83(1)	0.92(3)	0.82(1)	0.85(1)	0.95(1)	0.73(1)	0.76(1)	0.79(1)	0.81(2)	0.90(1)	0.93(1)	0.83(1)

Because of the problems associated with *model-free* fitting, we have chosen instead to investigate the behavior of the two linkages using our MD simulations. The correlation time for overall molecular tumbling was estimated by calculating the second-order orientational autocorrelation function, $C_{O2}(t)$, for a unit vector $\boldsymbol{u}$ "rigidly attached" to the disaccharide (eq 8, where P_2 is the Legendre polynomial described in section 2). In the case of maltose a unit vector aligned between C1 and C4′ was chosen, and for isomaltose, between C1 and C5′. For such a vector, the internal correlation $C_I(t)$ is identically unity; therefore, $C_{O2}(t)$ will have the same correlation time as the correlation function for overall motion. Plots of these functions for maltose

$$C_{O2}(t) = \langle P_2(u(0) \cdot u(t)) \rangle \tag{8}$$

and isomaltose are shown in Figure 2. The overall correlation time, τ_M, was estimated by fitting a single exponential $C_O(t) = \exp(-t/\tau_M)$ to the initial part of $C_{O2}(t)$ for each solution simulation. A value of 76 ps was found for maltose and 106, 109, and 80 ps for isomaltose from three separate simulations started from the three lowest minima on the adiabatic surface (simulations A, B, and C, respectively). The difference in τ_M between the isomaltose simulations is due to the drag that these different conformations have on the surrounding water molecules. The results for maltose and isomaltose are consistent with previous MD results for sucrose,[21] and experimental results for oligosaccharides of similar size.[43]

The contribution of internal motion toward molecular relaxation is estimated by calculating the root-mean-square fit (RMS) time correlation function (TCF) (eq 9), where $RMS(t_a,t_b)$ is the best RMS fit obtained between structures at times t_a and t_b using a standard fitting procedure.[44,45]

$$C(t) = \langle RMS(0,t) \rangle \tag{9}$$

Representative RMS fit autocorrelation functions for maltose and isomaltose in water are shown in Figure 2. It is not possible to calculate a value for τ_e directly from these functions as could be done for τ_M, but the time taken for all correlation to be lost is around 50−100 ps in each case. Notably, the initial relaxation in isomaltose is more rapid than in maltose, suggesting that its internal motions are more rapid. The effect of water on the internal RMS fit autocorrelation functions (not shown) is to slow their initial decay slightly and to damp out the high-frequency fluctuations relative to the vacuum case. The estimates obtained for internal and rotational correlation times illustrate that these occur on a similar time scale to that of molecular tumbling, which is problematic when applying the *model-free* formalism to the experimental data.

Order parameters were calculated using eq 6 from all of the solution simulations and are listed in Table 1. For both molecules, the values are relatively high, indicating that they are quite rigid; this is probably due to the inherent rigidity of the six-membered glucosyl monomer. The similarity in S^2 values within a ring supports this view. The generally lower order parameters found for the C6 and C6′ carbons as compared with those within the rings is evidence of their greater motional freedom. There is no significant difference between S^2 values of the rings in the case of maltose. However, the carbons on the reducing ring of isomaltose have lower order parameters as

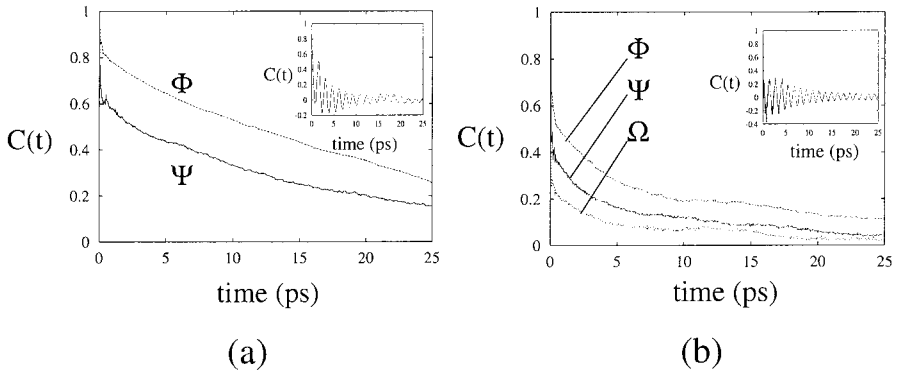

Figure 3. Time correlation functions of the fluctuations in glycosidic dihedral angles for (a) maltose and (b) isomaltose (from well A) in solution. The autocorrelation function of the phi dihedral fluctuations for the corresponding vacuum simulation is shown as an inset in each.

TABLE 2: Calculated and Experimental ^{13}C T_1 Relaxation Times for Maltose[38] at 5.9T (250 MHz) and Isomaltose at 9.4 T (400 MHz)

	C1	C2	C3	C4	C5	C6	C1′	C2′	C3′	C4′	C5′	C6′
						Maltose						
T_1(sim)	0.66	0.63	0.69	0.68	0.68	0.37	0.68	0.69	0.75	0.70	0.73	0.39
T_1(expt)	0.57	0.58	0.56	0.53	0.56	0.33	0.71	0.68	0.69	0.63	0.68	0.30
						Isomaltose						
T_1 (sim A)	0.55	0.56	0.61	0.60	0.60	0.30	0.59	0.64	0.70	0.62	0.66	0.32
T_1 (sim B)	0.52	0.52	0.57	0.56	0.56	0.28	0.52	0.52	0.56	0.54	0.54	0.28
T_1 (sim C)	0.69	0.70	0.76	0.75	0.74	0.40	0.71	0.75	0.81	0.79	0.78	0.38
T_1 (sim ave)	0.59	0.59	0.65	0.64	0.63	0.33	0.61	0.64	0.69	0.65	0.66	0.34
T_1 (expt.)	0.66(1)	0.55(2)	0.60(1)	0.58(1)	0.58(1)	0.37(1)	0.68(1)	0.65(1)	0.67(3)	0.64(2)	0.61(2)	0.34(1)

compared with those on the nonreducing ring. This may originate from a difference in flexibility between the Ω and Φ torsions.

Although it is difficult to obtain the value of τ_e from a *model-free* fit for small oligosaccharides without making assumptions, order parameters may still be estimated by setting τ_e to zero. The values of order parameters obtained from such a fit with $\tau_M = 0.1$ ns using the program MODELFREE[46,47] are also given in Table 1, and agree well with the simulated values. The T_1 relaxation times constitute a more direct comparison with experiment and may be calculated from the MD trajectories using eq 7. On the basis of the fit to the C_{O2} correlation functions, overall rotational correlation times of 76 and 100 ps were used for maltose and isomaltose, respectively. The results of this calculation together with the experimental values for the β-anomer are reported in Table 2. The agreement is generally good, with the same trend evident in both sets of data. The T_1's for the reducing ring are generally higher than those for the nonreducing ring in both experimental and simulated data sets. Benesi and Brant[38] proposed that anomeric exchange may be responsible for this; however, our model, which does not include this effect, is able to reproduce the trend. The difference in T_1 between the rings can therefore be explained by the difference in mobility of the two rings, evident in the order parameters. The T_1 values for the C6's are much lower than the others as a simple consequence of these carbons having two attached protons. The T_1 values for maltose are generally similar to that of isomaltose, which agrees well with the briefly reported results of Liu and Brant.[48]

Having considered the gross internal and overall correlation times, we now examine the mobility about each of the glycosidic angles. Figure 3 gives the correlation functions for the fluctuations in glycosidic dihedrals for the maltose simulation and the isomaltose simulation from well A. For maltose, the Φ and Ψ dihedrals have correlation times of around 20 ps, as opposed to about 5 ps for the Φ, Ψ, and Ω dihedrals of isomaltose. Therefore, fluctuation about these dihedrals occurs much more rapidly in isomaltose than maltose in solution. Moreover, the vacuum fluctuations about the same dihedrals (Figure 3, inset) are very similar for both molecules, suggesting that the difference is due to interactions with water. An interesting feature of the isomaltose dihedral correlation functions is the more rapid decay in correlation of the Ω torsion as compared with those of Φ and Ψ. This implies a greater flexibility in the former dihedral and is consistent with the observed differences in order parameters for the reducing and nonreducing sugar rings. Even though the internal motion and the tumbling rate are of the same order from our estimates of τ_e and τ_M, the dihedral correlation functions reveal a more rapid internal motion. These observations can be compared with those found for sucrose. While the *model free* parameters for internal and overall motion are of a similar magnitude,[20] nOe experiments reveal a rapid motion about the glycosidic linkage.[49] Poppe and van Halbeek pointed out rapid internal motion about the glycosidic bond is transparent to relaxation parameters including ^{13}C T_1.

5. Conformational Analysis

The maltose map reported elsewhere,[36] comprises a deep energy well at (Φ,Ψ) coordinates of (−50, −40) designated the *A well* and a smaller *C well* at (20, 20) with an interleading saddle point at (0,0). A minor *B well* at (−15,−15) is located in the same area as the A well. The maltose crystal structure[5] lies within this low energy region at (0,−13). Our maltose trajectory matches the results of extensive previous MD studies on maltose in solution in that it samples mainly the A well, and occasionally the B well (data not shown).[26,27,50] It was previously shown that the inclusion of water in the simulation allows the molecule to explore a greater range of conformational space than in a vacuum.[36,37]

As compared to maltose, isomaltose potentially has a much greater conformational space due to the extra bond in the glycosidic linkage. The effective three-dimensional adiabatic

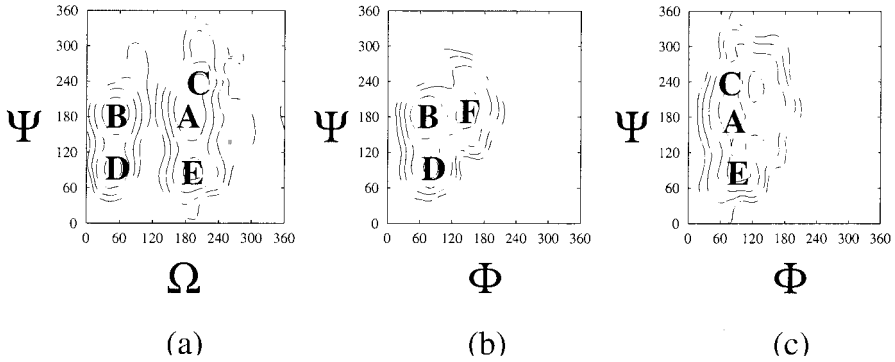

Figure 4. Representative two-dimensional sections from the isomaltose adiabatic map for (a) $\Phi = 80°$, (b) $\Omega = 60°$, and (c) $\Omega = 200°$. The positions of the six principal wells A−F are indicated.

TABLE 3: Six Lowest Lying Energy Minima on the Isomaltose Adiabatic Map

Φ	Ψ	Ω	label	energy (kcal/mol)
80	180	180	A	80.5415
80	180	60	B	80.9447
80	240	200	C	81.4936
80	100	40	D	81.8962
80	80	200	E	82.0833
140	180	60	F	82.3294

energy surface E(Φ,Ψ,Ω) for isomaltose revealed that all of the significant local minima in the adiabatic map for the α-(1→6)-linkage are located in a single low energy region. The six lowest wells were found, all within 2 kcal/mol of the global minimum. These have been labeled A to F, as listed in Table 3, and are illustrated by three representative two-dimensional slices in Figure 4a−c. All of the wells, except for F, have Φ close to 80° in accordance with the *exo*-anomeric effect, which causes polar substituents to be oriented away from the glucosyl ring. The network of minima lies in two sets, distinguished by having values of Ω close to either 60° (wells B,D,F) or 200° (wells A,C,E), with a relatively high energy penalty for transitions in Ω relative to Ψ (Figure 4a). The three sections shown in Figure 4 therefore provide a good illustration of the topology of the energy landscape. The barriers between the minima can be further rationalized though Newman projections down the three interresidue bonds as shown in Figure 5. The Φ and Ψ dihedrals each have only one 1,4-clash on transition between rotamers, while Ω has three (since both termini of the bond have three substituents). This is probably the main reason for the high energy barrier for Ω transitions relative to those in Ψ, whereas the exo-anomeric effect plays a dominant role in Φ transitions. The preferred conformers may be rationalized through these projections. The two gauche conformers in Φ compatible with the exo-anomeric effect ($\Phi \approx 60°, 180°$) can be distinguished from each other by observing that in the conformation with Φ close to 180° there is steric conflict between the C6 methylene and O2 on residue 1 that is not present in the other rotamer. Further, the minimum for Ψ is clearly 180°, as it best avoids clashes between C1 and the elements of ring 2. Likewise, most of the minima have their Ψ values close to the 180°. The favored values of Ω are the same *gg* and *gt* rotamers preferred by the free hydroxymethyl group. This preference has also been observed through vicinal NMR coupling constants for an α(1→6) linked tetrasaccharide.[51]

The molecular structures corresponding to the conformational minima A−F differ principally in the values of the three glycosidic dihedrals Φ, Ψ, and Ω with the notable exception of well C. All of wells A, B, D, E, and F have their secondary alcohols forming a clockwise hydrogen bond linked "crown"

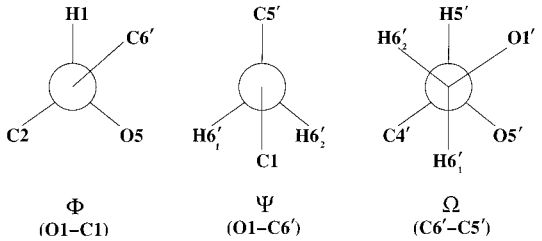

Figure 5. Newman projections of the three isomaltose α-(1→6) glycosidic dihedral angles.

on the nonreducing sugar (seen from above the ring), and an anticlockwise hydrogen bond linked "crown" on the reducing sugar while the hydroxymethyl group is *gg* in all, and the C5−C6−O6−H6 torsion is in the g^+ rotamer. Well C is the exception, having a different conformation for the nonreducing sugar, where the secondary alcohols form an anticlockwise crown, the hydroxymethyl is *gt* and the C5−C6−O6−H6 torsion is g^-. Despite being close in the adiabatic map, wells A and C are favored for different reasons. Well A is low in energy mainly as a consequence of having low steric strain associated with its glycosidic dihedrals. Hydrogen bonding does not appear to play an important part in the stability of well A, since most of the other minima display a similar extent of hydrogen bonding. However, well C forms several more hydrogen bonds in exchange for a slight deformation from the sterically ideal dihedrals of well A. The lack of interaction between the rings in most of the minima may be responsible for the greater flexibility about the α (1→6)-link seen from the dihedral angle TCF's described in section 4.

Conjugate peak refinement[52] is a method for calculating the lowest energy or saddle path between two states. The optimized reaction path between the four main minima (A, B, D, E) was calculated using CHARMM, following the cycle of paths (i), (ii), (iii), and (iv) shown in Figure 6a. The points between the minima in the adiabatic map were used as "seeds" in the calculation. The energy profile along the resulting reaction coordinate gives an indication of the energy barrier along the "ideal" path. Plots of the energy profiles for each transition are shown in Figure 6b. The barriers to rotation about Ψ, namely, for the A → E and D → B transitions, are less than 2 kcal in height sufficiently small to be crossed in a vacuum at 300 K. By contrast the transitions involving Ω rotations (i.e., B → A and E → D) require approximately 9 kcal to overcome the intervening barrier. Thus, the principle degree of freedom in the α(1→6)-linkage appears to be the Ψ dihedral, since rotation about Ω is energetically unfavorable for steric reasons and Φ is constrained by the *exo*-anomeric effect.

Finally, the form of our energy surface is compared with that previously calculated with the MM3 force-field[53] for isomaltose.

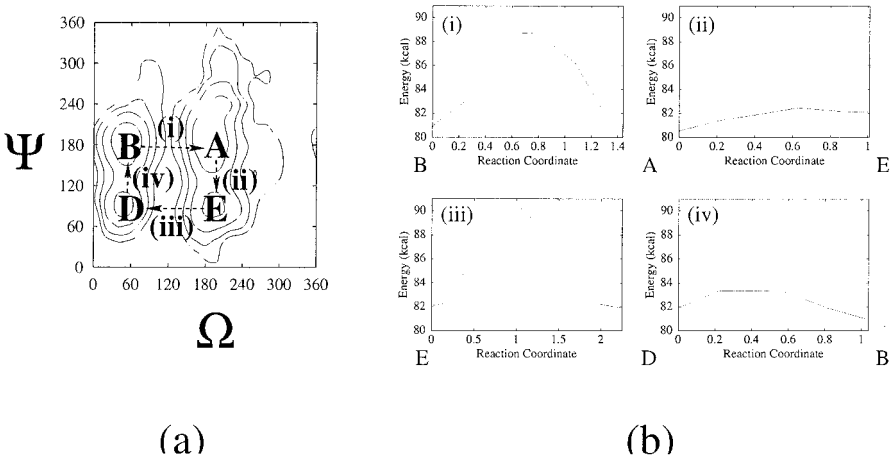

Figure 6. Characterizing isomaltose interwell transition pathways: (a) definition of transitions between wells illustrated on $\Phi = 80°$ section; (b) energy profiles (kcal/mol) along the reaction coordinate for each transition.

The two maps are qualitatively similar, in having Φ restricted to a similar range, although the MM3 surface includes low energy wells with Ω in the *tg* conformation which is not seen in the adiabatic surface produced by our force field and simulated annealing procedure. The presence of a *tg* conformation is not observed experimentally in other $\alpha(1\rightarrow6)$ linked oligosaccharides.[51] Nonetheless, wells A, B, D, and E from our map each correspond to one of the six lowest energy wells listed in the earlier study.

The conformations sampled by isomaltose in a vacuum and solution may be analyzed using the features of the adiabatic map. None of the six vacuum dynamics runs crossed the large energy barrier in Φ: however, transitions were observed from minima C and E to A and from D and F to B. The runs from wells A and B did not make any transitions, and in general, a very narrow range of dihedral space proximal to the minima was explored. Projections of the dihedral trajectories for the simulations from wells A and B in a vacuum are given in Figure 7a,c as illustration of this.

By contrast, the MD simulations with explicit solvent made more interwell transitions and explored a greater volume of conformational space. Projections of the dihedral trajectories for the solution runs from A and B in Figure 7b,d show that a broader region around the minima is sampled. Moreover, the solvent appears to have biased the simulation away from the vacuum minima in certain cases, such as well E (Figure 7b). This demonstrates that the water does indeed allow the disaccharide to explore wider regions of the vacuum adiabatic map, by allowing it to form alternate hydrogen bonds and thus reduce the energy of the transition states. The increased sampling of the saddle points in solution and the more gradual nature of the solution transitions support this interpretation.

The solution simulation from the C well was not distinguishable from that started from the A well, although the two minima were clearly observed as discrete populations in the vacuum run from the C well. Thus, the interresidue hydrogen bond that stabilized C in a vacuum is absent in solution.

6. Solution Structure

We have shown that explicitly included water damps the fluctuations in dihedrals differently for the $\alpha(1\rightarrow4)$- and $\alpha(1\rightarrow6)$-linked disaccharides (Figure 3) and enlarges the accessible conformational space (Figure 7). We would like to characterize in more detail the nature of the solute−solvent interaction to explain the plasticizing effect of the water.

TABLE 4: Hydrogen Bonding Statistics for Maltose and Isomaltose[a]

simulation initialization	solution			vacuum
	to water	bridging	internal	internal
maltose from saddle	1.08 (0.45)	0.14 (0.12)	0.23 (0.09)	0.38 (0.07)
isomaltose from A well	1.41 (0.46)	0.23 (0.14)	0.12 (0.05)	0.34(0.05)
isomaltose from B well	1.47 (0.45)	0.32 (0.13)	0.13 (0.07)	0.38(0.07)

[a] The unbracketed number refers to the average number of hydrogen bonds per sugar oxygen (as either donor or acceptor), while the numbers in brackets indicate the average lifetime in picoseconds of each such bond. Bridging hydrogen bonds in the solution dynamics are the subset of those to water in which the water molecule is in turn hydrogen bonded to another hydroxyl or other oxygen in the sugar molecule.

The interaction of carbohydrate solutes with water is frequently described in terms of the hydrogen bonds formed between the carbohydrate hydroxyls and the water molecules.[26,50] The directed nature of these bonds is believed to be responsible for the strong solvation effects observed in water. Hydrogen bonding statistics (average number of hydrogen bonds per sugar oxygen and average lifetime) are listed in Table 4 for the maltose simulations and selected isomaltose simulations.

Solvation reduces the average number of intramolecular (internal) hydrogen bonds per oxygen in all cases, because of competing interactions with water. The loss of intramolecular hydrogen bonds is greater for the isomaltose simulations than for maltose, which is compensated for by the larger number of bonds to water for the $\alpha(1\rightarrow6)$-linked sugar. On this simple basis, isomaltose appears to interact more strongly with the water. The higher average intramolecular hydrogen bonding of maltose in water may arise partly from the persistent interresidue hydrogen bond between O2 and O3′; an alternative bridging interaction through a water molecule ($O2-O_w$-O3′) is also possible. This particular arrangement has been previously observed and is postulated to be responsible for the helical structure of V-amylose.[36] Interresidue hydrogen bonds are absent from isomaltose, but there is good evidence for bridged hydrogen bonds between the residues in the folded B conformation: the average number of bridged hydrogen bonds to O2 is 0.65 and to O5′ is 0.56.

The hydrogen bonded interactions between water and the sugar solute induce a specific distribution of water about the solute in which water closer to the solute tends to be localized in certain high density regions relative to the "bulk" solvent

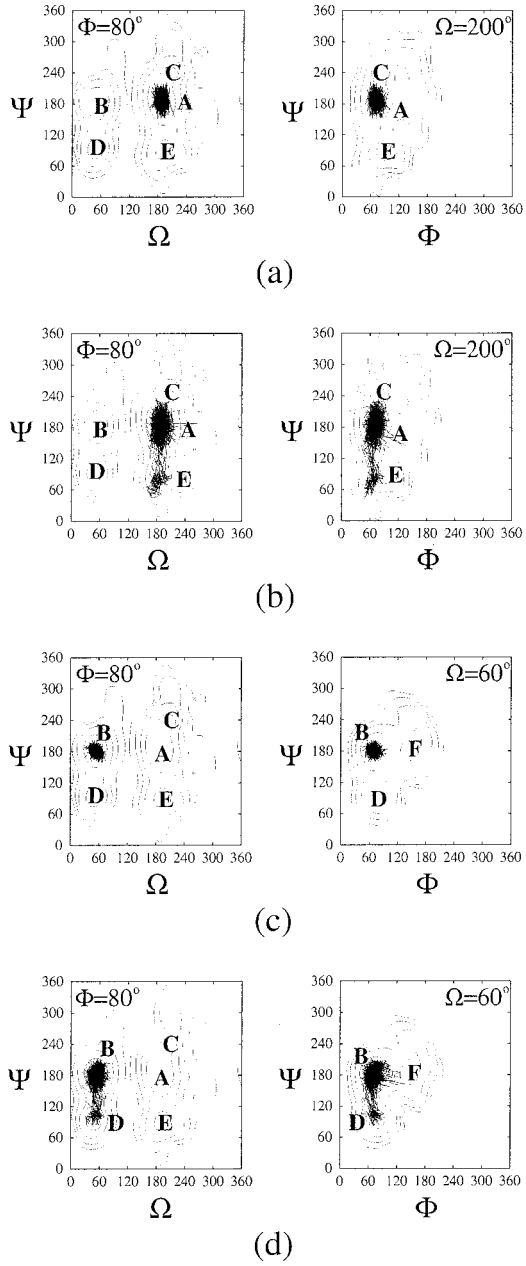

Figure 7. Projections of isomaltose MD trajectories onto adiabatic map sections: the glycosidic dihedral trajectories are plotted onto appropriate slices for the simulation from minimum A (a) in a vacuum and (b) in solution, and the simulation from minimum B (c) in a vacuum and (d) in solution.

further away. Radially averaged pair distribution functions (PDF) between each sugar oxygen and the water oxygens, $g(O_w)$,[54] provide approximate pictures of how the water structures about each oxygen site. The O3 oxygen is typical of most in having a strong first peak at 2.82 Å, which on integration over a sphere of radius 3.5 Å about the oxygen, results in a first shell of approximately 3.2 waters for each hydroxyl. This is much larger than the number of hydrogen bonded interactions calculated above (Table 4), so there is clearly significant local water density that is not participating in hydrogen bonds to the hydroxyls. The O5 oxygen has a more distant first peak in its PDF, corresponding to a weaker interaction with the water; the total integrated number of waters up to 3.5 Å is only 1.15. This structuring of the water about the sugar solute has also been shown by means of Voronoi analysis[36] and through analysis of the contribution of the solute−solvent contribution to the dielectric of the solution.[55]

The pair distribution function gives only approximate information about the nature of solvent structure about each disaccharide, as it is radially averaged: the position of the maximum is the same for all hydroxyls, although the maximum peak height may vary. Specific solute−solvent interactions, however, would be expected to give a complex directional distribution of water about each saccharide, which may not be revealed in the PDF. A more detailed picture may be obtained by calculating the full three-dimensional spatial distribution function.[36,56−59] This is done by averaging the water distribution about each disaccharide over the whole trajectory, after correcting for translational and rotational solute motion. Although maltose essentially samples a single large well comprising the A and B minima throughout the simulation, isomaltose adopts a number of discrete conformations (Figure 7). Averaging the solvent distribution over such slowly exchanging conformations could give rise to a more disperse distribution than would otherwise be obtained. The trajectory structures were therefore grouped using a clustering algorithm[60,61] according to their glycosidic and primary alcohol dihedrals. Water density distributions were calculated for the trajectory frames falling within a certain RMS distance of the structure closest to the center of each cluster. The distance was chosen so as to pick a similar number of frames to those assigned to the cluster by the original analysis. Such distributions are shown for the largest clusters for the maltose simulation ($\Phi = -27°$, $\Psi = -26°$) and the isomaltose simulation from well A ($\Phi = 71°$, $\Psi = 196°$, $\Omega = 194°$) in Figure 8a,b, respectively.

Common to both of the illustrated density distributions is the general pattern of water density around each ring. The peak of water density is generally located between the hydroxyls, supporting the contention that all of the hydroxyls participate in hydrogen bonded water bridges with their neighbors, albeit weakly. The isosurfaces are usually elongated perpendicular to the plane of the ring, with the peak densities being close the equatorial plane. The elongation can be interpreted as arising from those waters that are hydrogen bond donors, so only one of their hydrogens needs to be near the equatorial hydroxyls. The distance from these water oxygen peaks to the potentially hydrogen-bonded hydroxyl covers the full range of hydrogen bonding, from 2.4 to 3.4 Å. However, the interpretation of the maximum water oxygen density is not as straightforward as a simple preference for regions in which favorable contacts may be made with the solute (such as through hydrogen bonding) as several of the water peaks are more than 3.4 Å away from the nearest sugar hydroxyl. It appears therefore that the isomaltose solute has a capacity for structuring the water other than through direct hydrogen-bonded interactions. This could be either through secondary hydrogen bonding or through hydrophobic interactions.[36]

Despite the broad similarities in the water structure about the maltose and isomaltose solutes, it is clear that the water adopts a much more localized structure about maltose. The inherent rigidity of the maltose solute relative to isomaltose would contribute to this, as the water distribution would be averaged about a more restricted set of solute conformations. This greater flexibility of the isomaltose solute, allowing it to interact with water in a more heterogeneous way, helps explain the higher average number of hydrogen bonds it forms with solvent.

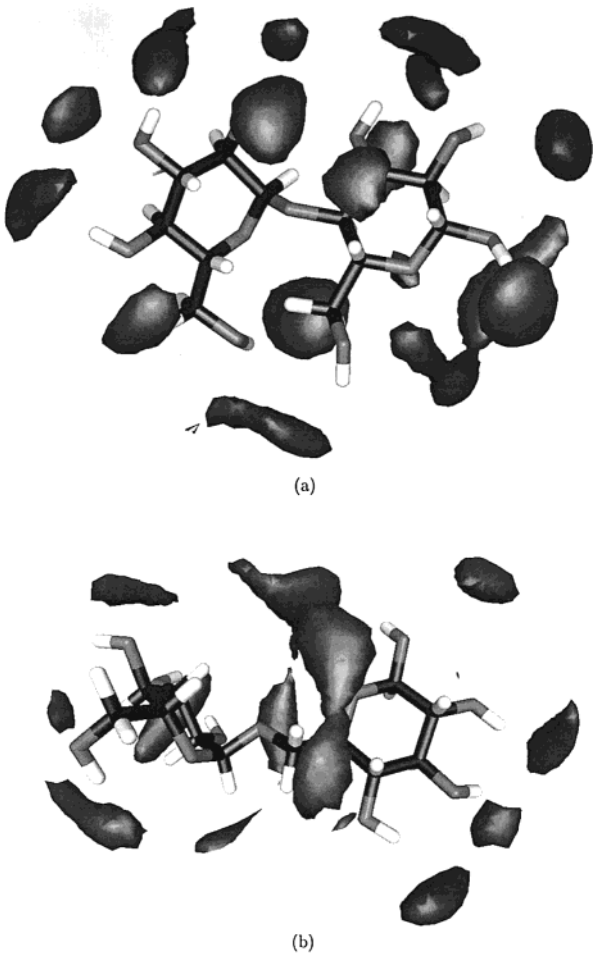

Figure 8. Plots of water density distribution about each disaccharide using isosurfaces 50% above bulk water density. The main cluster arising from the dynamics was used for each of (a) maltose and (b) isomaltose.

7. Conclusion

Our investigation of the dynamical properties and solution structure of the disaccharides maltose and isomaltose by molecular dynamics simulation illustrates the different motional properties of the α(1→4) and α(1→6) glycosidic linkages. In both cases, the overall and internal correlation times are similar (τ_M is around 76 ps for maltose and 100 ps for isomaltose, while τ_e is around 50−100 ps in each case). In this motional regime, the validity of a direct fit to the relaxation parameters is questionable, as these parameters have very little dependence on τ_e. From simulation, however, we were able to extract order parameters which indicate that while both disaccharides are conformationally restricted, isomaltose is slightly less so. The time dependence of dihedral fluctuations, as represented by their time correlation functions differs markedly between the linkages: the α(1→6) linkage has correlation times of 5 ps as compared with 20 ps for the α(1→4), even though their behavior in a vacuum is similar. A direct comparison with experiment, made by comparison of the measured and calculated longitudinal relaxation times, is good evidence for the validity of the simulation. The variation of the T_1 times computed from the three different isomaltose simulations shows that the limited sampling influences the calculated values. Ideally, these would be calculated from longer simulations with better sampling of configurational space.

A novel method for calculating the spatial distribution function (SDF) for the solvent about the saccharide, in which the solute structures are selected by cluster analysis to avoid averaging due to conformational exchange, has been used to calculate the SDFs for each disaccharide. Despite eliminating averaging between discrete conformations (corresponding to different wells in the adiabatic map), there remains evidence of a greater conformational distribution for isomaltose, resulting from its larger volume of accessible conformational space within a specific energy well. In addition, the extended structure of isomaltose appears to have a greater capacity for forming hydrogen bonds with the solvent.

Maltose and isomaltose are the simplest possible models for the α(1→4) and α(1→6) glycosidic linkages in amylopectin. From the results presented here, the greater flexibility of the α(1→6) linkage seems likely to play a role in the increased solubility of polysaccharides containing these linkages as compared with those polysaccharides in which they are absent. To test this, it will be necessary to study larger oligosaccharides containing both types of linkage to determine whether the predictions from these simple models will be generally applicable. We are presently investigating oligosaccharides of this type via NMR and computer simulations.[62]

Acknowledgment. This work was supported by the USDA-ARS Grant no. 58-4012-5-F120 and the Foundation for Research And Development (NRF Pretoria). We would like to thank Dr. J. L. Willet (USDA-ARS, Peoria IL laboratory) for helpful discussions.

Supporting Information Available: Table of T1 experimental data for isomaltose at three different field strengths. This material is available free of charge via the Internet at http://pubs.acs.org.

References and Notes

(1) Fukuda, M. *Cell Surface Carbohydrates: Cell-Type Specific Expression*; Fukuda, M., Ed.; Oxford University Press: Oxford, 1994, pp 2−52.
(2) Liu, Q.; Tompson, D. B. *Carbohydr. Res.* **1998**, *314*, 221−235.
(3) Doane, W. M. *Starch/Staerke* **1992**, *44*, 293−295.
(4) Shogren, R. L.; Fanta, G. L.; Doane, W. M. *Starch/Staerke* **1993**, *45*, 276−280.
(5) Quigley, G. J.; Sarko, A.; Marchessault, R. H. *J. Am. Chem. Soc.* **1970**, *92*, 5834−5839.
(6) Imberty, A.; Perez, S. *Carbohydr. Res.* **1988**, *181*, 41−55.
(7) Jeffrey, G. A. *Carbohydr. Res.* **1991**, *222*, 47−55.
(8) Hinrichs, W.; Buttner, G.; Steifa, M.; Betzel, C.; Zabel, V.; Pfannemuller, B.; Saenger, W. *Science* **1987**, *238*, 205−208.
(9) Imberty, A.; Buleon, A.; Perez, S. *Starch/Staerke* **1991**, *43*, 375−385.
(10) French, A. D.; Gardner, K. H. *Fiber Diffraction Methods*; American Chemical Society: Washington, DC, 1990; Vol. 141.
(11) Waigh, T. A.; Hopkinson, I.; Donald, A. M.; Butler, M. F.; Heidelbach, F.; Riekel, C. *Macromolecules* **1997**, *30*, 3813−3820.
(12) Ohtani, T.; Yoshino, T.; Ushiki, T.; Hagiwara, S.; Maekawa, T. *J. Elect. Micros.* **2000**, *49*, 487−489.
(13) Poppe, L. *J. Am. Chem. Soc.* **1993**, *115*, 8421−8426.
(14) Bock, K.; Duus, J. Q. *J. Carbohydr. Chem.* **1994**, *13*, 513−543.
(15) Rockwell, G. D.; Grindley, T. B. *J. Am. Chem. Soc.* **1998**, *120*, 10953−10963.
(16) van Halbeek, H. *Curr. Opin. Struct. Biol.* **1994**, *4*, 697−709.
(17) van Halbeek, H.; Sheng, S. *Prog. Biotech.* **1995**, *10*, 15−28.
(18) Rutherford, T. J.; Homans, S. W. *Biochemistry* **1994**, *33*, 9606−9614.
(19) Naidoo, K. J.; Denysyk, D.; Brady, J. W. *Protein Eng.* **1997**, *10*, 1249−1261.
(20) Engelsen, S. B.; Perez, S.; Braccini, I.; Du Penhoat, C. H. *J. Comput. Chem.* **1995**, *16*, 1096−1119.
(21) Engelsen, S. B.; du Penhoat, C. H.; Perez, S. *J. Phys. Chem.* **1995**, *99*, 13334−13351.
(22) Hardy, B. J.; Egan, W.; Widmalm, G. *Int. J. Biol. Macromol.* **1995**, *17*, 149−160.
(23) Xu, Q.; Mohan, S.; Bush, C. A. *Biopolymers* **1996**, *38*, 339−354.
(24) Lipari, G.; Szabo, A. *J. Am. Chem. Soc.* **1982**, *104*, 4559−4570.

(25) Lipari, G.; Szabo, A. *J. Am. Chem. Soc.* **1982**, *104*, 4546−4559.
(26) Brady, J. W.; Schmidt, R. K. *J. Phys. Chem.* **1993**, *97*, 958−966.
(27) Ha, S. N.; Madsen, L. J.; Brady, J. W. *Biopolymers* **1988**, *27*, 1927−1952.
(28) Palma, R.; Himmel, M. E.; Liang, G.; Brady, J. W. Molecular Mechanics Studies of Cellulases. In *ACS Symposium Series: Glycosyl Hydrolases in Biomass Conversion*; Himmel, M. E., Ed.; American Chemical Society: Washington, DC, 2001; Chapter 7, Vol. 769; pp 112−130.
(29) Brooks, B. R.; Bruccoleri, R. E.; Olafson, B. D.; States, D. J.; Swaminathan, S.; Karplus, M. *J. Comput. Chem.* **1983**, *4* (2), 187−217.
(30) Ha, S. N.; Giammona, A.; Field, M.; Brady, J. W. *Carbohydr. Res.* **1988**, *180*, 207−221.
(31) Jorgensen, W. L. *J. Am. Chem. Soc.* **1981**, *103*, 335−340.
(32) Jorgensen, W. L. *J. Phys. Chem.* **1982**, *77*, 4156−6516.
(33) Levy, R. M.; Karplus, R. M. *J. Am. Chem. Soc.* **1981**, *103*, 5998−6011.
(34) Kirkpatrick, S.; Gelatt, C. D.; Vecchi, M. P. *Science* **1983**, *220*, 671−680.
(35) Naidoo, K. J.; Brady, J. W. *Chem. Phys.* **1997**, *224*, 263−273.
(36) Naidoo, K. J.; Kuttel, M. M. *J. Comput. Chem.* **2001**, *22*, 445−456.
(37) Ott, K.; Meyer, B. *Carbohydr. Res.* **1996**, *281*, 11−34.
(38) Benesi, A. J.; Brant, D. A. *Macromolecules* **1984**, *18*, 1109−1116.
(39) Arnosti, C.; Repeta, D. J. *Starch/Staerke* **1995**, *47*, 73−75.
(40) McCain, D. C.; Markley, J. L. *J. Magn. Reson.* **1987**, *73*, 244−251.
(41) Kowalewski, J.; Widmalm, G. *J. Phys. Chem.* **1994**, *98*, 28−34.
(42) Maler, L.; Widmalm, G.; Kowalewski, J. *J. Phys. Chem.* **1996**, *100*, 17103−17110.
(43) Kjellberg, A.; Rundlof, T.; Kowalewski, J.; Widmalm, G. *J. Phys. Chem. B* **1997**, *102*, 1013−1020.
(44) Kabsch, W. *Acta Crystallogr. Sect. A* **1976**, *32*, 922−923.
(45) Kabsch, W. *Acta Crystallogr. Sect. A* **1978**, *34*, 827−828.
(46) Palmer, A. G.; Rance, M.; Wright, P. E. *J. Am. Chem. Soc.* **1991**, *113*, 4371−4380.
(47) Mandel, A. M.; Akke, M.; Palmer, A. G. *J. Mol. Biol.* **1995**, *246*, 144−163.
(48) Liu, H.-S.; Brant, D. A. *Abstr. Pap. − Am. Chem. Soc.* **1995**, *209*, 100-CARB.
(49) Poppe, L.; van Halbeek, H. *J. Am. Chem. Soc.* **1992**, *114*, 1092−1094.
(50) Astley, T.; Birch, G. G.; Drew, M. G. B.; Rodger, P. M. *J. Phys. Chem. A.* **1999**, *103*, 5080−5090.
(51) Imberty, A.; Perez, S.; Hricovíni, M.; Shah, R. N.; Carver, J. P. *Int. J. Biol. Macromol.* **1993**, *15*, 17−23.
(52) Fischer, S.; Karplus, M. *Chem. Phys. Lett.* **1992**, *194*, 252−261.
(53) Dowd, M. K.; Reilly, P. J.; French, A. D. *Biopolymers* **1994**, *34*, 625−638.
(54) Brady, J. W. *J. Am. Chem. Soc.* **1989**, *111*, 5155−5164.
(55) Höchtl, P.; Boresch, S.; Steinhauser, O. *J. Chem. Phys.* **2000**, *112*, 9810−9821.
(56) Kusalik, P. G.; Svishchev, I. M. *Science* **1994**, *265*, 1219−1221.
(57) Svishchev, I. M.; Kusalik, P. G. *J. Chem. Phys.* **1993**, *99*, 3049−3059.
(58) Vishnyakov, A.; Widmalm, G.; Kowalewski, J.; Laaksonen, A. *J. Am. Chem. Soc.* **1999**, *121*, 5403−5412.
(59) Lui, Q.; Brady, J. W. *J. Am. Chem. Soc.* **1996**, *118*, 12276−12286.
(60) Karpen, M. E.; Tobias, D. J.; Brooks, C. L., III. *Biochemistry* **1993**, *32*, 412−420.
(61) Carpenter, G. A.; Grossberg, S. *Appl. Opt.* **1987**, *26*, 4919−4930.
(62) Naidoo, K. J.; Best, R. B.; Jackson, G. E. *Abstr. Pap. − Am. Chem. Soc.* **2000**, *220*, 15-CARB.